

Article

Sn-Doped Hydrated V₂O₅ Cathode Material with Enhanced Rate and Cycling Properties for Zinc-Ion Batteries

Kai Guo ^{1,2}, Wenchong Cheng ¹, Haiyuan Liu ¹, Wenhao She ¹, Yinpeng Wan ¹, Heng Wang ¹, Hanbin Li ¹, Zidan Li ¹, Xing Zhong ¹, Jinbo Ouyang ^{1,*} and Neng Yu ^{1,*}

¹ Jiangxi Province Engineering Research Center of New Energy Technology and Equipment, School of Chemistry, Biology and Materials Science, East China University of Technology, Nanchang 330013, China

² State Key Laboratory of Materials Processing and Die & Mould Technology, Huazhong University of Science and Technology, Wuhan 430074, China

* Correspondence: oyjb1001@163.com (J.O.); neng063126@ecut.edu.cn (N.Y.)

Abstract: Water molecules and cations with mono, binary, and triple valences have been intercalated into V₂O₅ to significantly improve its electrochemical properties as a cathode material of zinc-ion batteries. Sn as a tetravalent element is supposed to interact aggressively with the V₂O₅ layer and have a significant impact on the electrochemical performance of V₂O₅. However, it has been rarely investigated as a pre-intercalated ion in previous works. Hence, it is intriguing and beneficial to develop water molecules and Sn co-doped V₂O₅ for zinc-ion batteries. Herein, Sn-doped hydrated V₂O₅ nanosheets were prepared by a one-step hydrothermal synthesis, and they demonstrated that they had a high specific capacity of 374 mAh/g at 100 mA/g. Meanwhile, they also showed an exceptional rate capability with 301 mAh/g even at a large current density of 10 A/g, while it was only 40 mAh/g for the pristine hydrated V₂O₅, and an excellent cycling life (87.2% after 2500 cycles at 5 A/g), which was far more than the 25% of the pure hydrated V₂O₅. The dramatic improvement of the rate and cycling performance is mainly attributed to the faster charge transfer kinetics and the enhanced crystalline framework. The remarkable electrochemical performance makes the Sn-doped hydrate V₂O₅ a potential cathode material for zinc-ion batteries.

Keywords: vanadium pentoxide; cathode; doping; rate performance; stability



Citation: Guo, K.; Cheng, W.; Liu, H.; She, W.; Wan, Y.; Wang, H.; Li, H.; Li, Z.; Zhong, X.; Ouyang, J.; et al. Sn-Doped Hydrated V₂O₅ Cathode Material with Enhanced Rate and Cycling Properties for Zinc-Ion Batteries. *Crystals* **2022**, *12*, 1617. <https://doi.org/10.3390/cryst12111617>

Academic Editor: Sergio Brutti

Received: 7 October 2022

Accepted: 8 November 2022

Published: 11 November 2022

Publisher's Note: MDPI stays neutral with regard to jurisdictional claims in published maps and institutional affiliations.



Copyright: © 2022 by the authors. Licensee MDPI, Basel, Switzerland. This article is an open access article distributed under the terms and conditions of the Creative Commons Attribution (CC BY) license (<https://creativecommons.org/licenses/by/4.0/>).

1. Introduction

Aqueous zinc-ion batteries (ZIBs), as one of the candidates for next-generation rechargeable batteries, have attracted tremendous interest because their zinc metal anodes have some unique features, including a high theoretical capacity (819 mA h/g), a low redox potential (−0.76 V vs. SHE), a small radius (0.74 Å), and the two-electron reaction of Zn/Zn²⁺ [1–5]. Unfortunately, the relatively large radius (4.3 Å) of the hydrated Zn²⁺ ion in an aqueous electrolyte and a strong electrostatic interaction with the cathode host both add to a high energy barrier for its intercalation/deintercalation in the cathode materials, resulting in sluggish electrochemical kinetics, serious electrochemical polarization, as well as unsatisfied cycling and rate performances [6–10]. Therefore, it is crucial to design and develop suitable cathode materials for constructing high-performance ZIBs [3,11,12].

A variety of cathode materials have been investigated, such as manganese-based oxides, Prussian blue analogs, conducting polymers, and vanadium-based oxides, over the past few years [13–17]. Among these cathode materials, the vanadium-based oxides have been widely studied for ZIBs because of their multivalence, open skeleton structure, and high theoretical capacities [13,14,18–21]. Vanadium pentoxide (V₂O₅) is one of the promising materials due to its high theoretical capacity and layered structure with it having a large interspace [1,3,22,23]. However, V₂O₅ usually displays a low conductivity, a poor ion diffusion coefficient, a long activation process, and an unsatisfying cyclic stability [1,24–26].

Generally, the nanostructures with high specific surface areas and short ion diffusion paths are conducive to good Zn^{2+} diffusion rates and rapid electrochemical kinetics [27]. Additionally, recent research suggests that the pre-insertion of water molecules or foreign metal ions (e.g., Na^+ and Ca^{2+}) into V_2O_5 not only strongly modifies its crystal structure, but it also plays an important role in its electrochemical kinetics [28–30]. The water molecules intercalated in the V_2O_5 interlayers pillar its layered structure and effectively function like a “lubricant” to facilitate fast Zn^{2+} transport, significantly improving the rate and cycle performance of V_2O_5 [31].

As another choice, metal ions incorporated between the V_2O_5 layers may covert the crystal structure of V_2O_5 to a more stable tunnel framework or enlarge the interlayer spacing and strongly bond to the apical oxygens of the V_2O_5 layers to maintain the structural stability of V_2O_5 , depending on radiuses and charges of the metal ions [7,32]. Cations with mono, binary, and triple valences, such as Na, K, Mg, Ca, Zn, Mn, and Fe, have already been studied [10,11,28,33]. Generally, multivalent metal ions with a higher charge density and stronger electrostatic interaction than those of the monovalent cations are beneficial to build a stronger bond with the vanadium oxide layers, resulting in a better structural stability and cycling performance [5]. Meanwhile, the strong electrostatic interaction between the V_2O_5 host and the foreign cations shields the interaction between the oxygen atom and Zn^{2+} and thus, it reduces the energy barrier of the Zn^{2+} diffusion inside V_2O_5 , which is conducive to a better rate performance [27]. However, the charge numbers of the doped metal ions are no more than three. What will happen to the zinc-ion storage capability if alien ions with a charge number of more than three are hybridized with V_2O_5 is unsure. The element tin, which is commonly in a tetravalent state with ion Sn^{4+} and with a charge number of four, is believed to interact more strongly with the V_2O_5 layer than other previously reported elements do, and it will have a significant impact on the electrochemical performance of V_2O_5 if it is doping V_2O_5 . However, it has been rarely investigated as a pre-intercalated ion in previous works. Hence, it is interesting and worthwhile to develop Sn-doped V_2O_5 cathodes for ZIBs and to clarify the role of the doped Sn element on the zinc-ion storage capability.

Herein, Sn-doped hydrated V_2O_5 was synthesized in a one-step hydrothermal method to realize a cathode material with a superior Zn-storage performance by a hydrothermal reaction. Compared with the pristine V_2O_5 , the obtained SnVO displays larger interlayer spacing, a greatly improved rate performance, and a superior cycling stability. SnVO delivers a high reversible specific capacity of 374 mAh/g at a current density of 100 mA/g, retains 320 mAh/g at 5000 mA/g, and maintains 87.5% of its initial capacity after cycling at 2 A/g for 2000 times. The facile synthesis route and its significant electrochemical performance enhancement suggest that Sn doping is an effective strategy and Sn-doped hydrated V_2O_5 is a prospective cathode materials for zinc-ion batteries.

2. Experimental Section

2.1. Preparation of Sn Doped $\text{V}_2\text{O}_5 \cdot n\text{H}_2\text{O}$

Two mmol of V_2O_5 (Sinopharm Chemical, Shanghai, China) and 0.2 mmol of $\text{SnCl}_4 \cdot 5\text{H}_2\text{O}$ (Adamas-beta, Shanghai, China) were dissolved in a mixture of 20 mL of deionized water and 10 mL H_2O_2 (30 wt%, Sinopharm Chemical, Shanghai, China) by magnetic stirring at room temperature. Then, the solution was poured into the autoclave reactor and heated at 200 °C for 48 h. The resulting reactants were vacuum filtered, thoroughly washed with deionized water, and then, they were dried at 80 °C for 6 h to obtain a dark red, dry gel, which was labeled as SnVOH. For the comparison, a sample was synthesized following the same procedure without the addition of $\text{SnCl}_4 \cdot 5\text{H}_2\text{O}$, and it was labeled as VOH.

2.2. Materials Characterizations

The crystalline structure of the samples was identified using an X'Pert 3 diffractometer (PANalytical, Almelo, The Netherlands) at the range from 5 to 80°. The morphologies and structure of the samples were investigated using a field emission scanning electron micro-

scope (FESEM, HITACHI SU8200, Tokyo, Japan) equipped with an energy-dispersive X-ray (EDX) detector and transmission electron microscopy (TEM, FEI Talos S-FEG). X-ray photoelectron spectroscopy (XPS, PHI QUANTERA-II SXM) was used to identify the valence state of the samples.

2.3. Electrochemical Measurements

The obtained SnVOH or VOH were mixed with a carbon nanotube (CNT) solution (10 mg/mL, XFNANO, Nanjing, China) and then, it was filtered using a cellulose film (0.22 μm , Shanghai Xinya, Shanghai, China) to form freestanding composite films, for which the mass ratios of SnVOH or VOH were 70%. Additionally, the as-prepared composite films were cut into small pieces and used directly as the cathode to assemble the CR2025 button cells in the air with metallic zinc foil (100 μm thick) as the anode, 3 M zinc trifluoromethane sulfonate ($\text{Zn}(\text{CF}_3\text{SO}_3)_2$) solution as the electrolyte, and glass fiber as the separator. Cycle voltammetry (CV) was performed on the button cells using an electrochemical workstation (CHI 660E, CH Instruments, Inc., Bee Cave, TX, USA) within the potential range of 0.2–1.7 V vs. Zn/Zn^{2+} . The electrochemical impedance spectra (EIS) were acquired with the same electrochemical workstation over the frequency range of 0.01– 10^5 Hz at a voltage of 5 mV. Additionally, galvanostatic charge–discharge (GCD) tests and galvanostatic intermittent titration technique (GITT) tests were carried out using a NEWARE 4000 system (Neware Technology Limited, Shenzhen, China) at room temperature. For the GITT test, the coin cell was charging/discharging for 20 min at 0.1 A/g with a 120 min relaxation duration. The solid diffusion coefficient was calculated according to the equation below:

$$D = \frac{4L^2}{\pi\tau} \left(\frac{\Delta E_s}{\Delta E_t} \right)^2 \quad (1)$$

where t , τ , and ΔE_s represent the duration of the current pulse (s), the relaxation time (s), and the steady-state voltage change (V) that was induced by the current pulse, respectively [34]. ΔE_t is the voltage change (V) during the galvanostatic current pulse after eliminating the IR drop. L is the ion diffusion length (cm) of the electrode, which was equal to the thickness of the composite film electrode (40.2 and 41.7 μm for the VOH and SnVOH composite film, respectively). The specific capacity, the energy density, and the power density were calculated based on the mass of active materials from the cathode.

3. Results and Discussion

The VOH and SnVOH were both synthesized via a facile hydrothermal reaction, as shown in Figure S1. The compositions of the as-prepared samples were characterized by XRD and XPS. No peaks related to tin metal or tin oxides were detected, and there are only six discrete peaks in the XRD pattern for both VOH and SnVOH, corresponding to the (00n) planes of a hydrated V_2O_5 phase (JCPDS NO. 40–1297) (Figure 1a), which is similar to previous research [35]. Additionally, there are slight blue shifts which occurred at the characteristic peaks of VOH after doping the Sn element, suggesting that the (00n) interlayer spacing of VOH was expanded through the Sn doping. The expanded interlayer spacing is commonly induced by the volume change after introducing doping ions to the interlayers of the V-O bilayers in the hydrated V_2O_5 [1,3]. According to the Bragg Equation in the Supporting Information file, the calculated interplanar distances of the (001) plane are $d_{001} = 14.91$ and 14.81 \AA for SnVOH and VOH, respectively. The small differences in the interplanar distance of two samples could be ascribed to a combination of two factors. On one hand, the intercalated Sn^{4+} can lead to an expanded interlayer spacing. On the other hand, the strong attraction between the intercalated Sn^{4+} ions and the adjacent V-O bilayers tends to bring the V-O bilayers close to or narrow to the interlayer spacing. These two factors counteract each other and they induce a small interplanar distance change [7,32]. The schematic crystalline structure of SnVOH is illustrated in Figure S2. In the XPS spectrum of SnVOH (Figure 1b), two pairs of characteristic peaks can be found in the V 2p spectra; the stronger peaks at 516.9 and 524.4 eV are ascribed to V^{5+} ,

and the weaker peaks at 516.0 and 522.8 eV are from V^{4+} , respectively [36]. The weak peaks from V^{4+} indicate a very small amount of V^{4+} , which may be caused by the doping of Sn^{4+} . The two O1s XPS peaks are deconvoluted into (V-O) lattice oxygen at 530.4 eV and a hydroxyl (V-OH) of defective oxygen at 532.1 eV, respectively. The peaks that can be observed in the Sn 3d spectrum belong to Sn^{4+} (Figure 1c), confirming the successful doping of the Sn element in the SnVOH [37].

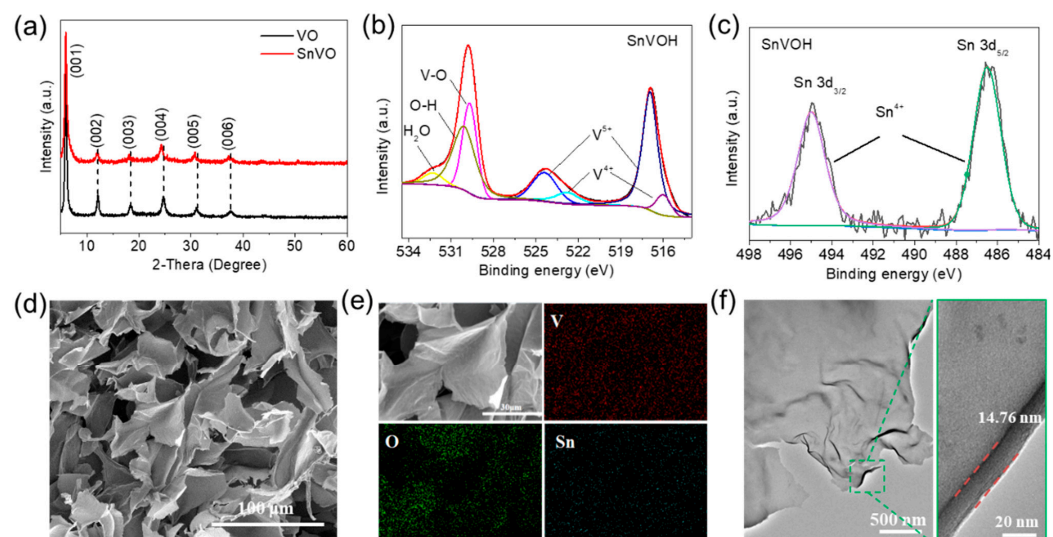


Figure 1. Characterization of SnVOH. (a) XRD patterns of SnVOH sample; (b) XPS spectra of (b) O1s and V 2p and (c) Sn 3d; (d) SEM of SnVOH sample; (e) EDS mapping of SnVOH sample; (f) TEM of SnVOH sample.

SEM and TEM were performed to observe the morphology and structure of SnVOH. The SEM image (Figure 1d) shows that the SnVOH sample is composed of nanosheets with lateral sizes of tens of micrometers, and the VOH sample has a similar morphology with an even element distribution (Figure S3). The diagram in Figure 1e shows the uniform distribution of the V, O, and Sn elements. Additionally, the EDS elemental analysis result demonstrates that the molar ratio of the Sn element in the SnVOH accounts for 3.85%, as shown in Table S1. The TEM image of SnVOH in Figure 1f confirms the nanosheet morphology and demonstrates that the thickness of the nanosheets is in the range of 10–20 nanometers. The distribution of the elements Sn, V, and O in the SnVOH nanosheet was characterized by the EDS. The above analysis results suggest the Sn-doped V_2O_5 has been successfully synthesized.

To evaluate the zinc-ion storage performance, VOH and SnVOH were mixed with the CNT solution and then, they filtered to form free-standing composite films, which were cut into small pieces and used directly as the cathode. The VOH and SnVOH nanosheets were both evenly mixed with the CNTs (Figure S4a,c), and the composite films were layered at a thickness of 40.2 and 41.7 μm , respectively (Figure S4b,d). The coin cells were assembled using the VOH and SnVOH-based cathodes and tested in the voltage range of 0.2–1.7 V vs. Zn/Zn^{2+} . There are two pairs of redox peaks in the CV profile of the VOH-based cathode, as shown in Figure S5a. Similarly, the CV profile of SnVOH in Figure 2a shows two oxidation peaks at 0.75 and 1.11 V along with two reduction peaks at 0.37 and 0.75 V, which correspond to the multi-step extraction/insertion of the Zn^{2+} ion in the framework of SnVOH, respectively [37,38]. The redox reactions are consistent with the plateaus of the initial three galvanostatic charge and the discharge curves of SnVOH at 0.1 A/g in Figure 2b. The GCD profiles of SnVOH in Figure 2c show the maximum discharge capacity is 387 mAh/g at a current density of 0.1 A/g. Additionally, its capacity retention is impressive, at 77.8%, when the current density increases from 0.1 to 10 A/g. The pristine VOH shows an average discharge capacity of 395 mAh/g at

0.1 A/g (Figure 2d), which is close to that of SnVOH. However, its rate performance is unsatisfactory by possessing a dramatically lower retention of 12.6% when the current density increased to 10 A/g. The average discharge capacities of 387, 365, 349, 348, 345, 330, 321, 309, and 301 mAh/g were recorded for SnVOH at the current densities of 0.1, 0.3, 0.5, 0.8, 1, 3, 5, 8, and 10 A/g, respectively (Figure 2d). SnVOH had higher capacities than VOH did at the current densities over 0.5 A/g, and the capacity advantage is larger at a higher current density. The significant improvement in the rate performance of SnVOH can be accounted for by the highly facilitated Zn^{2+} diffusion in the VOH framework after incorporating the Sn element. Not only is there a dramatically enhanced rate performance, but SnVOH also demonstrates an improved electrochemical stability at both the small and large current densities, as shown in Figure 2e,f, respectively. During the cycling test at 10 A/g for 500 cycles, the capacity of SnVOH goes through a slow increasing process during the initial 100 cycles and then, it remains stable in the following cycles, while the capacity of VOH decays rapidly in the first 10 cycles, then, it slowly increases in the following 200 cycles, and stays steady in the last 300 cycles. The capacity retentions for SnVOH and VOH are 135.4% and 76.1% after the cycling at 10 A/g for 500 times, respectively (Figure 2e). During the cycling at 5 A/g for 2500 cycles, the VOH cathode undergoes fast capacity fading, leading to a final capacity retention of 24%, which is much lower than the 71% of the SnVOH cathode in the same condition (Figure 2f). In addition, the rate and cycling performance of the Sn-doped hydrated V_2O_5 is superior to the results from the recent research on hydrated V_2O_5 , as shown in Table S2. The rapid capacity decay of VOH may be mainly attributed to the unstable layered structure and the dissolution of VOH during repeated insertion/extraction of zinc ions. Additionally, the enhanced cycling performance of SnVOH reveals the outstanding structural stabilizer function of the doped Sn ions.

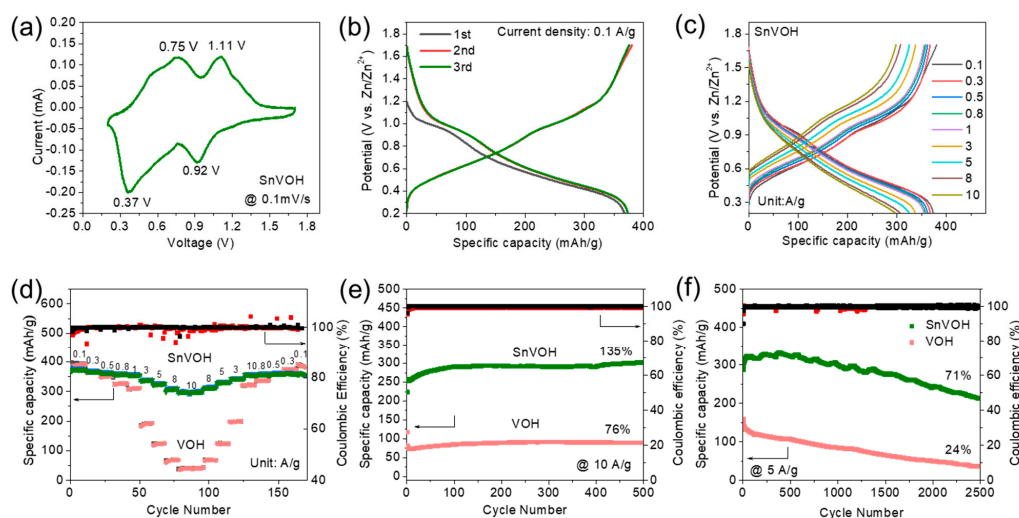


Figure 2. Electrochemical performance of VOH and SnVOH. (a) C–V curves at 0.1 mV/s in the voltage range of 0.2–1.7 V vs. Zn^{2+}/Zn , (b) corresponding GCD curves, (c) representative galvanostatic charge–discharge curves at different current densities, (d) rate capacities at current densities between 0.1 to 10 A/g, (e) cycling performance at 10 A/g and (f) cycling performance at 5 A/g for the VOH and SnVOH sample.

The high-rate performance and long-term stability of the SnVOH cathode are substantially controlled by the electrochemical kinetics, which were analyzed through the C–V curves at different scanning rates and during the GITT test, as shown in Figure 3. The C–V curves of SnVOH in Figure 3a maintain a similar shape with two pairs of charge and discharge peaks, while the reduction peaks and oxidation peaks shift to lower and higher

voltages at increased scan rates, respectively. The peak current (i) and scan rate (v) have a relationship that is defined by the following equations [39]:

$$I = av^b \quad (2)$$

which can be transformed to

$$\log(i) = b \log(v) + \log(a) \quad (3)$$

where a and b are the variables. The b value ranges from 0.5 to 1.0, which indicates a different mechanism. A b value of one is indicative of the dominated contribution of the surface capacitance to the total capacity, and a b value of 0.5 exhibits diffusion-controlled charge storage [27]. In addition, the slope of the $\log(i)$ versus the $\log(v)$ plot can be used to estimate the b value, as shown in Figure 3b,c. The b values of the peaks 1–4 for the SnVOH electrode are 0.97, 0.81, 0.93, and 0.89, (Figure 3b), which implies the SnVOH has considerable kinetics, and its charge storage mainly comes from surface capacitance, and it is slightly influenced by the diffusion process. By fitting the $C-V$ curves at different scan rates in Figure S5b, the b values of the peaks 1–4 for the VOH electrode are 0.85, 0.86, 0.72, and 0.96 (Figure S5c), suggesting the capacity of the VOH cathode is also influenced by both the capacitive and diffusion processes, and it is dominated by the surface capacitive capacity. Furthermore, the capacity is divided as a capacitive-controlled part (k_1v) and diffusion-induced part ($k_2v^{1/2}$) which are described by the following equations [40]:

$$i = k_1v + k_2v^{1/2} \quad (4)$$

or

$$i/v^{1/2} = k_1v^{1/2} + k_2 \quad (5)$$

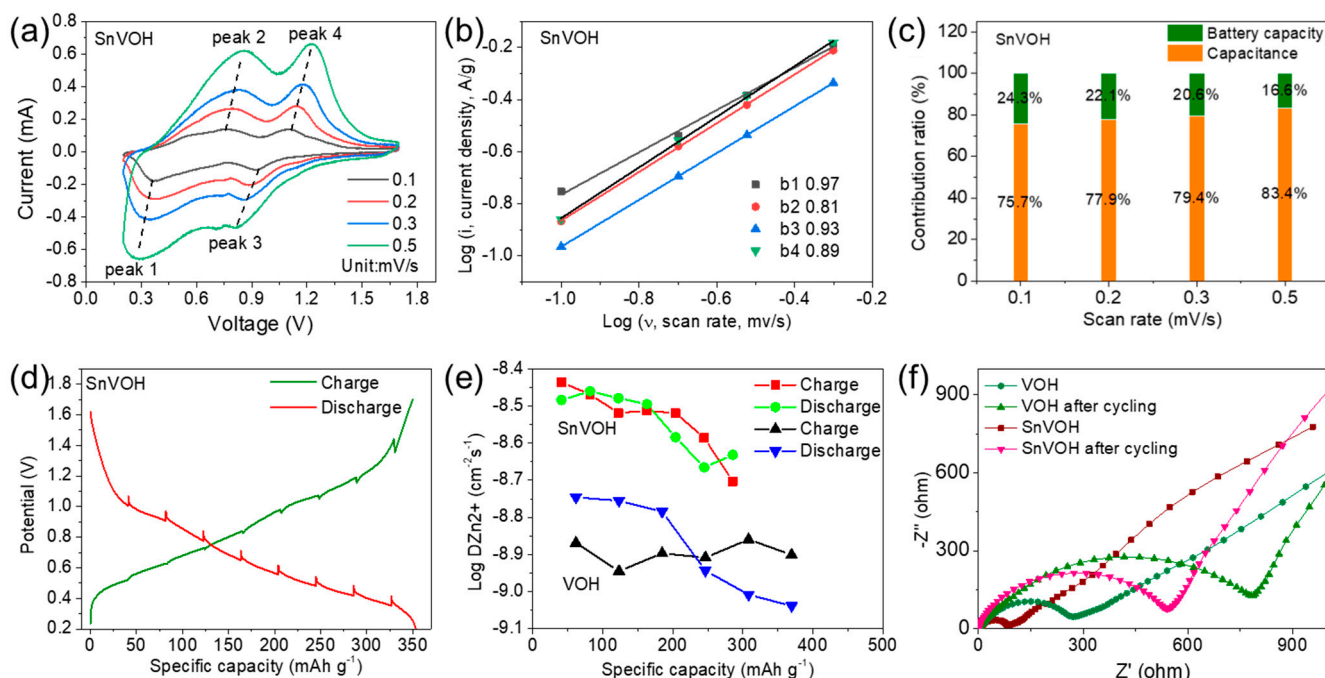


Figure 3. Kinetics study of VOH and SnVOH. (a) $C-V$ curves of SnVOH electrode at different scan rates, (b) $\log(\text{current})$ vs. $\log(\text{scan rate})$ plots of four peaks in $C-V$ curves during the cycles, and (c) capacity contribution ratios of battery type capacity and capacitance, (d) the discharge/charge curves in GITT measurement of SnVOH, (e) corresponding diffusivity coefficient of Zn^{2+} in discharge and charge processes of SnVOH samples, and (f) electrochemical impedance profiles recorded for the VOH and SnVOH electrodes before electrochemical tests and after cycling at 5 A/g for 2500 times.

The ratios of the surface-controlled capacitive and the diffusion-induced parts of SnVOH at various scan rates are displayed in Figure 3c. The surface-controlled capacitive contribution ratio increases from 75.7% (0.1 mV/s) to 83.4% (0.5 mV/s), indicating that the batteries possess fast charge-transfer kinetics. For VOH, the surface-controlled capacitive contribution ratio is 21.5% (0.1 mV/s), and this increases to 36.3% (0.5 mV/s), as presented in Figure S5d. The much higher surface-controlled capacitive contribution ratio for SnVOH implies that it has much faster kinetics when one is doping the Sn element, which may be ascribed to the effect of Sn⁴⁺ shielding the interaction between the oxygen atom and Zn²⁺ [41].

Then, the constant current intermittent titration technique (GITT) was used to determine the ion diffusion coefficient of Zn²⁺ in the VOH and SnVOH cathodes (Figures S5e and S3d). As demonstrated in Figure 3e, the diffusion coefficients of SnVOH are from 10^{-8.9} to 10^{-8.6}/(cm² s) during the charge and discharge processes, respectively, which are higher than those of the VOH samples (10^{-9.0} to 10^{-8.8}/(cm² s), in Figure S5f). The results confirm that Zn²⁺ migration in SnVOH is faster when it is compared to that in VOH. Thus, the much higher rate performance of SnVOH can be ascribed to a reduced interfacial impedance and an enhanced ion diffusion. Moreover, doping the Sn element largely reduces the charge transfer resistance from 300 to 100 Ω (Figure 3f), which is indicative of a reduced ion diffusion impedance between the interface of the cathode and electrolyte. After cycling at 5 A/g for 2500 times, the charge transfer resistance of SnVOH-based cell rises to about 580 Ω, which is still smaller than 880 Ω of VOH based cell. The results confirm that faster electrochemical kinetics can be achieved by doping the Sn element.

4. Conclusions

In summary, the Sn-doped hydrated V₂O₅ ZIB cathode materials were prepared by simple one-step hydrothermal synthesis. Compared to the undoped sample, the Sn-doped hydrated V₂O₅ demonstrates a significant enhancement in its rate performance and cyclic stability. SnVOH shows a high initial reversible capacity of 387 mAh/g at 0.1 A/g, an excellent rate capability with 301 mAh/g even at a large current density of 10 A/g, and it retains 87.5% of its initial capacity after the cycling at 2 A/g for 2000 times. The rate and cycling performance of Sn-doped hydrated V₂O₅ are superior to the results from recent research on hydrated V₂O₅. These great improvements can be due to the smaller charge transfer resistance and the higher zinc diffusion coefficient that occur after the Sn doping. Therefore, this work reveals that Sn doping is an effective strategy to improve the zinc storage performance of hydrated V₂O₅, and the Sn-doped hydrated V₂O₅ is a promising cathode material candidate to construct ZIBs of a high specific capacity, an excellent rate performance, and a high durability.

Supplementary Materials: The following supporting information can be downloaded at: <https://www.mdpi.com/article/10.3390/cryst12111617/s1>, Figure S1: Scheme of synthesis of SnVOH; Figure S2: The schematic crystalline structure of SnVOH; Figure S3: EDS characterization of VOH sample; Table S1: The molar ratio of different elements in SnVOH; Figure S4: Characterization of VOH and SnVOH composite cathodes; Figure S5: Electrochemical characterization of VOH-based cathode; Table S2. Electrochemical performance comparison of SnVOH with recent literature data on doped hydrated V₂O₅-based cathodes in ZIBs. Refs. [42–45] are cited in the Supplementary Materials file.

Author Contributions: Conceptualization, K.G. and N.Y.; investigation, W.C. and H.L. (Haiyuan Liu); validation, H.L. (Haiyuan Liu), W.S. and Y.W.; writing—original draft preparation, K.G.; writing—review and editing, N.Y. and J.O.; visualization, H.W., H.L. (Hanbin Li) and Z.L.; supervision, N.Y.; project administration, K.G.; funding acquisition, K.G., X.Z. and N.Y. All authors have read and agreed to the published version of the manuscript.

Funding: This research was funded by the National Natural Science Foundation of China (52102214, 51702048, and 22166003), the Jiangxi Provincial Natural Science Foundation (20202BAB213008, 20202BABL213003, and 20202BABL203026), the Opening Project of Jiangxi Province Engineering Research Center of New Energy Technology and Equipment (JXNE2021-04, JXNE2021-05), State Key Laboratory of Materials Processing and Die & Mould Technology, Huazhong University of Science and Technology (P2022-009), and the National (Jiangxi Province) College Students Innovation and Entrepreneurship Training Program 2020 (S202110405018, S202010405031 and S202010405018) supported this work.

Institutional Review Board Statement: Not applicable.

Acknowledgments: The authors would like to thank Xiaoming Chen from Shiyanjia Lab (www.shiyanjia.com) for the material characterization.

Conflicts of Interest: The authors declare no conflict of interest.

References

1. Ming, F.; Liang, H.; Lei, Y.; Kandambeth, S.; Eddaoudi, M.; Alshareef, H.N. Layered $Mg_xV_2O_5 \cdot nH_2O$ as Cathode Material for High-Performance Aqueous Zinc Ion Batteries. *ACS Energy Lett.* **2018**, *3*, 2602–2609. [[CrossRef](#)]
2. Pan, Q.; Dong, R.; Lv, H.; Sun, X.; Song, Y.; Liu, X.-X. Fundamental understanding of the proton and zinc storage in vanadium oxide for aqueous zinc-ion batteries. *Chem. Eng. J.* **2021**, *419*, 129491. [[CrossRef](#)]
3. Pang, Q.; He, W.; Yu, X.; Yang, S.; Zhao, H.; Fu, Y.; Xing, M.; Tian, Y.; Luo, X.; Wei, Y. Aluminium pre-intercalated orthorhombic V_2O_5 as high-performance cathode material for aqueous zinc-ion batteries. *Appl. Surf. Sci.* **2021**, *538*, 148043. [[CrossRef](#)]
4. Qi, Z.; Xiong, T.; Chen, T.; Shi, W.; Zhang, M.; Ang, Z.W.J.; Fan, H.; Xiao, H.; Lee, W.S.V.; Xue, J. Harnessing oxygen vacancy in V_2O_5 as high performing aqueous zinc-ion battery cathode. *J. Alloy. Compd.* **2021**, *870*, 159403. [[CrossRef](#)]
5. Qiu, N.; Yang, Z.; Xue, R.; Wang, Y.; Zhu, Y.; Liu, W. Toward a High-Performance Aqueous Zinc Ion Battery: Potassium Vanadate Nanobelts and Carbon Enhanced Zinc Foil. *Nano Lett.* **2021**, *21*, 2738–2744. [[CrossRef](#)]
6. Lübke, M.; Ning, D.; Armer, C.F.; Howard, D.; Brett, D.J.L.; Liu, Z.; Darr, J.A. Evaluating the Potential Benefits of Metal Ion Doping in SnO_2 Negative Electrodes for Lithium Ion Batteries. *Electrochim. Acta* **2017**, *242*, 400–407. [[CrossRef](#)]
7. Song, H.; Liu, C.; Zhang, C.; Cao, G. Self-doped V^{4+} - V_2O_5 nanoflake for 2 Li-ion intercalation with enhanced rate and cycling performance. *Nano Energy* **2016**, *22*, 1–10. [[CrossRef](#)]
8. Sun, R.; Qin, Z.; Liu, X.; Wang, C.; Lu, S.; Zhang, Y.; Fan, H. Intercalation Mechanism of the Ammonium Vanadate ($NH_4V_4O_{10}$) 3D Decussate Superstructure as the Cathode for High-Performance Aqueous Zinc-Ion Batteries. *ACS Sustain. Chem. Eng.* **2021**, *9*, 11769–11777. [[CrossRef](#)]
9. Suresh, R.; Giribabu, K.; Manigandan, R.; Munusamy, S.; Kumar, S.P.; Muthamizh, S.; Stephen, A.; Narayanan, V. Doping of Co into V_2O_5 nanoparticles enhances photodegradation of methylene blue. *J. Alloy. Compd.* **2014**, *598*, 151–160. [[CrossRef](#)]
10. Wang, H.; Ye, W.; Yang, Y.; Zhong, Y.; Hu, Y. Zn-ion hybrid supercapacitors: Achievements, challenges and future perspectives. *Nano Energy* **2021**, *85*, 105942. [[CrossRef](#)]
11. Song, M.; Tan, H.; Chao, D.; Fan, H.J. Recent Advances in Zn-Ion Batteries. *Adv. Funct. Mater.* **2018**, *28*, 1802564. [[CrossRef](#)]
12. Wang, H.; Jing, R.; Shi, J.; Zhang, M.; Jin, S.; Xiong, Z.; Guo, L.; Wang, Q. Mo-doped $NH_4V_4O_{10}$ with enhanced electrochemical performance in aqueous Zn-ion batteries. *J. Alloy. Compd.* **2021**, *858*, 158380. [[CrossRef](#)]
13. Fu, Q.; Wang, J.; Sarapulova, A.; Zhu, L.; Missyul, A.; Welter, E.; Luo, X.; Ding, Z.; Knapp, M.; Ehrenberg, H.; et al. Electrochemical performance and reaction mechanism investigation of V_2O_5 positive electrode material for aqueous rechargeable zinc batteries. *J. Mater. Chem. A* **2021**, *9*, 16776–16786. [[CrossRef](#)]
14. Geng, H.; Cheng, M.; Wang, B.; Yang, Y.; Zhang, Y.; Li, C.C. Electronic Structure Regulation of Layered Vanadium Oxide via Interlayer Doping Strategy toward Superior High-Rate and Low-Temperature Zinc-Ion Batteries. *Adv. Funct. Mater.* **2019**, *30*, 1907684. [[CrossRef](#)]
15. He, Z.; Jiang, Y.; Zhu, J.; Li, Y.; Jiang, Z.; Zhou, H.; Meng, W.; Wang, L.; Dai, L. Boosting the performance of $LiTi_2(PO_4)_3/C$ anode for aqueous lithium ion battery by Sn doping on Ti sites. *J. Alloy. Compd.* **2018**, *731*, 32–38. [[CrossRef](#)]
16. Kuang, M.; Han, P.; Huang, L.; Cao, N.; Qian, L.; Zheng, G. Electronic Tuning of Co, Ni-Based Nanostructured (Hydr)oxides for Aqueous Electrocatalysis. *Adv. Funct. Mater.* **2018**, *28*, 1804886. [[CrossRef](#)]
17. Liu, R.; Liang, Z.; Gong, Z.; Yang, Y. Research Progress in Multielectron Reactions in Polyanionic Materials for Sodium-Ion Batteries. *Small Methods* **2018**, *3*, 1800221. [[CrossRef](#)]
18. Kim, J.; Lee, S.H.; Park, C.; Kim, H.S.; Park, J.H.; Chung, K.Y.; Ahn, H. Controlling Vanadate Nanofiber Interlayer via Intercalation with Conducting Polymers: Cathode Material Design for Rechargeable Aqueous Zinc Ion Batteries. *Adv. Funct. Mater.* **2021**, *31*, 2100005. [[CrossRef](#)]
19. Ni, S.; Liu, J.; Chao, D.; Mai, L. Vanadate-Based Materials for Li-Ion Batteries: The Search for Anodes for Practical Applications. *Adv. Energy Mater.* **2019**, *9*, 1803324. [[CrossRef](#)]
20. Venkatesan, R.; Bauri, R.; Mayuranathan, K.K. Zinc Vanadium Oxide Nanobelts as High-Performance Cathodes for Rechargeable Zinc-Ion Batteries. *Energy Fuels* **2022**, *36*, 7854–7864. [[CrossRef](#)]

21. Li, R.; Xing, F.; Li, T.; Zhang, H.; Yan, J.; Zheng, Q.; Li, X. Intercalated polyaniline in V_2O_5 as a unique vanadium oxide bronze cathode for highly stable aqueous zinc ion battery. *Energy Storage Mater.* **2021**, *38*, 590–598. [[CrossRef](#)]
22. Lv, T.-T.; Liu, Y.-Y.; Wang, H.; Yang, S.-Y.; Liu, C.-S.; Pang, H. Crystal water enlarging the interlayer spacing of ultrathin $V_2O_5 \cdot 4VO_2 \cdot 2.72H_2O$ nanobelts for high-performance aqueous zinc-ion battery. *Chem. Eng. J.* **2021**, *411*, 128533. [[CrossRef](#)]
23. Tang, B.; Zhou, J.; Fang, G.; Guo, S.; Guo, X.; Shan, L.; Tang, Y.; Liang, S. Structural Modification of V_2O_5 as High-Performance Aqueous Zinc-Ion Battery Cathode. *J. Electrochem. Soc.* **2019**, *166*, A480–A486. [[CrossRef](#)]
24. Moretti, A.; Giuli, G.; Trapananti, A.; Passerini, S. Electrochemical and structural investigation of transition metal doped V_2O_5 sono-aerogel cathodes for lithium metal batteries. *Solid State Ion.* **2018**, *319*, 46–52. [[CrossRef](#)]
25. Wu, S.; Liu, S.; Hu, L.; Chen, S. Constructing electron pathways by graphene oxide for V_2O_5 nanoparticles in ultrahigh-performance and fast charging aqueous zinc ion batteries. *J. Alloy. Compd.* **2021**, *878*, 160324. [[CrossRef](#)]
26. Yu, H.; Rui, X.; Tan, H.; Chen, J.; Huang, X.; Xu, C.; Liu, W.; Yu, D.Y.; Hng, H.H.; Hoster, H.E.; et al. Cu doped V_2O_5 flowers as cathode material for high-performance lithium ion batteries. *Nanoscale* **2013**, *5*, 4937–4943. [[CrossRef](#)]
27. Yang, Y.; Tang, Y.; Fang, G.; Shan, L.; Guo, J.; Zhang, W.; Wang, C.; Wang, L.; Zhou, J.; Liang, S. Li^+ intercalated $V_2O_5 \cdot nH_2O$ with enlarged layer spacing and fast ion diffusion as an aqueous zinc-ion battery cathode. *Energy Environ. Sci.* **2018**, *11*, 3157–3162. [[CrossRef](#)]
28. Sheng, X.; Li, Z.; Cheng, Y. Electronic and Thermoelectric Properties of V_2O_5 , MgV_2O_5 , and CaV_2O_5 . *Coatings* **2020**, *10*, 453. [[CrossRef](#)]
29. Xu, X.; Xiong, F.; Meng, J.; Wang, X.; Niu, C.; An, Q.; Mai, L. Vanadium-Based Nanomaterials: A Promising Family for Emerging Metal-Ion Batteries. *Adv. Funct. Mater.* **2020**, *30*, 1904398. [[CrossRef](#)]
30. Zhang, X.; Dong, M.; Xiong, Y.; Hou, Z.; Ao, H.; Liu, M.; Zhu, Y.; Qian, Y. Aqueous Rechargeable Li^+ / Na^+ Hybrid Ion Battery with High Energy Density and Long Cycle Life. *Small* **2020**, *16*, e2003585. [[CrossRef](#)]
31. Zhu, K.; Wu, T.; van den Bergh, W.; Stefik, M.; Huang, K. Reversible Molecular and Ionic Storage Mechanisms in High-Performance $Zn_{0.1}V_2O_5 \cdot nH_2O$ Xerogel Cathode for Aqueous Zn-Ion Batteries. *ACS Nano* **2021**, *15*, 10678–10688. [[CrossRef](#)] [[PubMed](#)]
32. Shao, Y.; Sun, Z.; Tian, Z.; Li, S.; Wu, G.; Wang, M.; Tong, X.; Shen, F.; Xia, Z.; Tung, V.; et al. Regulating Oxygen Substituents with Optimized Redox Activity in Chemically Reduced Graphene Oxide for Aqueous Zn-Ion Hybrid Capacitor. *Adv. Funct. Mater.* **2020**, *31*, 2007843. [[CrossRef](#)]
33. Han, L.; Dong, S.; Wang, E. Transition-Metal (Co, Ni, and Fe)-Based Electrocatalysts for the Water Oxidation Reaction. *Adv. Mater.* **2016**, *28*, 9266–9291. [[CrossRef](#)] [[PubMed](#)]
34. Liao, M.; Wang, J.; Ye, L.; Sun, H.; Wen, Y.; Wang, C.; Sun, X.; Wang, B.; Peng, H. A Deep-Cycle Aqueous Zinc-Ion Battery Containing an Oxygen-Deficient Vanadium Oxide Cathode. *Angew. Chem. Int. Ed.* **2020**, *59*, 2273–2278. [[CrossRef](#)]
35. Wang, H.; Bi, X.; Bai, Y.; Wu, C.; Gu, S.; Chen, S.; Wu, F.; Amine, K.; Lu, J. Open-Structured $V_2O_5 \cdot nH_2O$ Nanoflakes as Highly Reversible Cathode Material for Monovalent and Multivalent Intercalation Batteries. *Adv. Energy Mater.* **2017**, *7*, 1602720. [[CrossRef](#)]
36. Du, Y.; Wang, X.; Sun, J. Tunable oxygen vacancy concentration in vanadium oxide as mass-produced cathode for aqueous zinc-ion batteries. *Nano Res.* **2020**, *14*, 754–761. [[CrossRef](#)]
37. Li, Y.; Yao, J.; Uchaker, E.; Zhang, M.; Tian, J.; Liu, X.; Cao, G. Sn-Doped V_2O_5 Film with Enhanced Lithium-Ion Storage Performance. *J. Phys. Chem. C* **2013**, *117*, 23507–23514. [[CrossRef](#)]
38. Wu, C.; Zhu, G.; Wang, Q.; Wu, M.; Zhang, H. Sn-based nanomaterials: From composition and structural design to their electrochemical performances for Li- and Na-ion batteries. *Energy Storage Mater.* **2021**, *43*, 430–462. [[CrossRef](#)]
39. Li, Z.; Zhang, C.; Liu, C.; Fu, H.; Nan, X.; Wang, K.; Li, X.; Ma, W.; Lu, X.; Cao, G. Enhanced Electrochemical Properties of Sn-doped V_2O_5 as a Cathode Material for Lithium Ion Batteries. *Electrochim. Acta* **2016**, *222*, 1831–1838. [[CrossRef](#)]
40. He, D.; Peng, Y.; Ding, Y.; Xu, X.; Huang, Y.; Li, Z.; Zhang, X.; Hu, L. Suppressing the skeleton decomposition in Ti-doped $NH_4V_4O_{10}$ for durable aqueous zinc ion battery. *J. Power Sources* **2021**, *484*, 229284. [[CrossRef](#)]
41. Byeon, Y.W.; Ahn, J.P.; Lee, J.C. Diffusion Along Dislocations Mitigates Self-Limiting Na Diffusion in Crystalline Sn. *Small* **2020**, *16*, e2004868. [[CrossRef](#)] [[PubMed](#)]
42. Wu, F.; Wang, Y.; Ruan, P.; Niu, X.; Zheng, D.; Xu, X.; Gao, X.; Cai, Y.; Liu, W.; Shi, W.; et al. Fe-doping enabled a stable vanadium oxide cathode with rapid Zn diffusion channel for aqueous zinc-ion batteries. *Mater. Today Energy* **2021**, *21*, 100842. [[CrossRef](#)]
43. Zhao, H.; Fu, Q.; Yang, D.; Sarapulova, A.; Pang, Q.; Meng, Y.; Wei, L.; Ehrenberg, H.; Wei, Y.; Wang, C.; et al. In Operando Synchrotron Studies of NH_4^+ Preintercalated $V_2O_5 \cdot nH_2O$ Nanobelts as the Cathode Material for Aqueous Rechargeable Zinc Batteries. *ACS Nano*. **2020**, *14*, 11809–11820. [[CrossRef](#)] [[PubMed](#)]
44. Xu, G.; Liu, X.; Huang, S.; Li, L.; Wei, X.; Cao, J.; Yang, L.; Chu, P.K. Freestanding, Hierarchical, and Porous Bilayered $Na_xV_2O_5 \cdot nH_2O$ / rGO / CNT Composites as High-Performance Cathode Materials for Nonaqueous K-Ion Batteries and Aqueous Zinc-Ion Batteries. *ACS Appl. Mater. Interfaces* **2020**, *12*, 706–716. [[CrossRef](#)] [[PubMed](#)]
45. Jiang, H.; Zhang, Y.; Xu, L.; Gao, Z.; Zheng, J.; Wang, Q.; Meng, C.; Wang, J. Fabrication of $(NH_4)_2V_3O_8$ nanoparticles encapsulated in amorphous carbon for high capacity electrodes in aqueous zinc ion batteries. *Chem. Eng. J.* **2020**, *382*, 122844. [[CrossRef](#)]